Assessment of humidity self-regulation functionality for ceramic tiles

J. Castellano, V. Sanz, E. Cañas, E. Sánchez

Instituto de Tecnología Cerámica (ITC), Universitat Jaume I (UJI), Castellón, Spain

Javier Castellano*
Email: javier.castellano@itc.uji.es
Telephone number: (+34) 964342424
Fax number: (+34) 964342425

Vicente Sanz
Email: sanzs@uji.es

Eugeni Cañas
Email: eugeni.canas@itc.uji.es

Enrique Sánchez
Email: enrique.sanchez@itc.uji.es

Abstract

The development of ceramic tiles with humidity regulating capacity is a topic of great interest for the comfort of interior spaces. The humidity regulating capacity of fired specimens from five compositions used for porous ceramic products has been assessed and their microstructure has been characterised. The main novelty of the work consists of obtaining pieces with regulating functionality from common ceramic raw materials used in industrial practice, establishing a kinetic model and confirming the role of porosity and microstructure.

The results have shown that moisture adsorption and desorption curves fit very well to a pseudo-second order model. Additionally, it has been found that the humidity regulating capacity is not related to the total porosity, but it depends on the presence of mesopores in the structure of the pieces. Concerning the tested compositions, those containing gibbsite present higher regulating capacity as a consequence of their greater amount of mesopores.

Keywords: ceramic compositions, moisture adsorption, kinetic model, capillary condensation, mesopores.

1 Introduction

Current demands for environmental comfort in indoor spaces require the use of air conditioning systems in buildings to regulate climatic conditions and maintain an approximately constant temperature. In order to reduce energy consumption, it is necessary to control the introduction of air from the outside, whose thermal characteristics are often different from those desired. This implies the development of more airtight and better thermally insulated buildings, which can lead to detrimental humidity conditions and reduced air quality. Inadequate humidity and poor air quality are associated with sick building syndrome and other allergic pathologies [1], [2]. In general, the relative humidity range in which a person feels comfortable is between 40 and 70 % [3]. Studies indicate that the reproduction of viruses and certain allergic sources such as mites, bacteria and moulds decreases when the humidity is maintained in this range [4], [5].

The humidity level of an indoor space is determined by the sources of humidity, the transport of humidity by air exchange with the outside and the exchange of humidity with the elements of the enclosure itself, such as the interior finish and objects, as it has been known that certain materials such as wood or paper have hygroscopic properties [6]. Typical methods for regulating the humidity of an interior space are based on mechanical devices, such as air conditioners or humidifiers, which consume significant amounts of energy. However, the ideal solution to this problem, from the point of view of energy saving and sustainable development, is the technology of self-regulation of indoor humidity by the building materials themselves [7].

The humidity regulating capacity of a material is defined by the Kelvin equation, which relates the relative vapour pressure required for capillary condensation to the radius of curvature of the pores [8]. From the Kelvin equation, taking into account the formation of a surface layer by adsorption prior to capillary condensation, Arai et al. [9], determined a pore size of 3.2 nm for a relative humidity of 40 % and 7.4 nm for a relative humidity of 70 %. However, other researches indicate that materials with pore sizes in the entire mesopore range (2-50 nm) have an effective ability to regulate humidity [10], [11]. In addition, studies show that mesoporous materials have the ability to adsorb formaldehyde and other volatile organic compounds thus contributing to enhance ceramic tile functionality in buildings [12], [13].

Materials with the ability to regulate humidity for ceramic tiles were initially studied and developed in Japan. Such materials, used in walls, floors and ceilings, have the ability to control indoor humidity by adsorbing and desorbing water vapour depending on changes in the relative humidity of the air [7], [14].These materials have attracted a great deal of attention because they can decrease the environmental load due to their zero-energy consumption. Thus, it has been shown that these materials can reduce energy consumption in buildings by 5 to 30 % [15]. However, the composition of these ceramic tiles with the new functionality relied on a specific raw material, allophane, which is a main constituent of volcanic soils in certain regions of Japan. Allophane, is an amorphous aluminium silicate clay mineraloid characterised by a porous structure with many small pores (mesopores). This feature gives this material the innate ability to regulate humidity which, more interestingly, is preserved after a typical ceramic firing cycle [16], [17].

Nevertheless, allophane is not an available raw material on the European continent, where there is a significant ceramic tile manufacturing industry (Spain and Italy are two of the world's main tile producers), therefore it is not surprising that attempts have been made in recent years to emulate the moisture regulating capacity of this mineral by using other more common natural or synthetic raw materials [18], [19]. Certain materials are known to have the ability to regulate humidity such as lime mortars [20], amorphous fumed silica [21], silica gel [22], some bio-composites [23] or zeolite-based materials [24]. Unfortunately, most of these solutions do not match ceramic processing requirements because these materials hardly preserve their unfired porous structure after a standard firing cycle. Recently, materials providing highly porous structures or high specific surface area after a firing process have attracted interest as ceramic materials with potential humidity regulating capacity. Thus, natural raw materials such as clayey marls, calcite, dolomite, diatomite and sepiolite or synthetic materials as gibbsite have been used to design ceramic compositions targeting the self-regulating humidity functionality [19], [25-28]. Most of these studies have addressed to develop highly porous fired microstructures without analysing the role of the different pore sizes or the reversibility of the humidity adsorption-desorption process. In addition, kinetic aspects of the phenomenon have not been addressed either.

In order to understand the moisture regulating functionality of ceramic materials with high porosity, the present research is proposed. The assessment of the capability of ambient humidity regulation with compositions used to produce porous materials in the ceramic sector in Southern Europe will contribute to the development of tiles with such functionality. Moisture regulation has been related to the porous microstructure, mainly, quantity and size of mesopores. Adsorption and desorption kinetics have also been analysed by proposing a behavioural model.

2 Experimental procedure

2.1 Materials and sample preparation

The analysis of the functionality has been carried out on five ceramic compositions of different nature, named C1 to C5. Table 1 shows descriptions and uses of the selected compositions. All of them are used at industrial level for the manufacture of porous ceramics by means of different processing strategies and compositions. Besides, C5 is a

variation of C4 in which the amount of gibbsite has been increased up to more than 50 wt% in the starting composition. The gibbsite content of composition C4 is higher than 40 wt%.

Table 1. Description and use of the five compositions studied in this research

Reference	Description	Use
C1	Spray-dried powder containing marly clay	Manufacture of porous wall tiles
C2	Clayey marl	Manufacture of bricks and roof tiles
C3	Spray-dried powder of dolomite-base composition	Manufacture of earthenware ceramics
C4	Spray-dried powder of gibbsite-base composition	Manufacture of advance porous ceramics for cosmetic application
C5	A modification of C4 with higher gibbsite content	Manufacture of advance porous ceramics for cosmetic application

The samples were in powder form except for raw material C2 which was ground to adapt the particle size to the requirements of the pressing process. For each composition, 40 mm diameter cylindrical specimens were prepared by uniaxial pressing following the industrial practice. Based on that, materials were wetted to a moisture content of 5.5 % on a dry basis and pressed at 300 $kg \cdot cm^{-2}$, except C1 and C2 which were pressed at 170 $kg \cdot cm^{-2}$. All the pressed bodies were fully dried in a laboratory oven at 110 ºC. Subsequently, the pressed specimens were fired in a laboratory electric furnace following a conventional firing cycle: a rapid heating ramp at 70 $ºC \cdot min^{-1}$ up to 500 ºC, a ramp at 25 $ºC \cdot min^{-1}$ from 500 ºC to maximum temperature and a dwell time of 6 minutes at maximum temperature. Due to breakage problems, the C4 bodies were fired more slowly with a ramp at 5 $ºC \cdot min^{-1}$ to maximum temperature. The maximum temperatures were in the range 1020-1120 °C depending on the typical temperatures used in the industrial practice. It should be borne in mind that too high a temperature causes excessive sintering of the part with loss of porosity while too low a temperature gives rise to mechanical strength problems due to lack of sintering. Lee et al. [27], have found that the moisture

adsorption capacity of humidity regulating ceramic materials decreases with increasing firing temperature.

2.2 Samples characterisation

The powdery samples were analysed for chemical and mineralogical composition. The chemical composition was characterised by wavelength dispersive X-ray fluorescence spectrometry (XRF; Axios, Panalytical). The identification of crystalline structures was carried out by X-ray diffraction (XRD; D8 Advance diffractometer, Bruker Theta-theta), obtaining the corresponding diffractograms from which the mineralogical species present were identified.

The laboratory fired pieces were characterised by determining the following properties: bulk density, linear shrinkage and water absorption. Bulk density was measured by Archimedes method. Linear shrinkage was calculated dimensionally from the difference between the dried and fired diameters of the specimens measured with a calliper, defining this parameter on a dry basis. Water absorption was determined by the boiling method, measuring the weight gain experienced by the specimens when placed in boiling water for a period of 2 hours.

The moisture adsorption and desorption tests were carried out in a climatic chamber (HC2020, Heraeus Vötsch) that allows regulating the temperature and relative humidity conditions, keeping the temperature constant during the whole test and modifying the relative humidity according to convenience. Initially, the specimens were placed inside the chamber, the temperature was set at 23 ºC and the relative humidity at 50 % for sufficient time to reach equilibrium with a minimum of 16 hours. Then, the pieces were extracted from the chamber, weighed (m_0) and reintroduced into the chamber. At that point, the temperature was maintained at 23 ºC, while the relative humidity was increased to 90 %. Finally, weighings were performed at different time periods (m_t) for 24 hours or until equilibrium was reached. The incremental amount of water adsorbed for each time period (q_t) was calculated as a percentage from equation 1. The equilibrium moisture content (q_e) was defined from equation 1 when the incremental amount of water does not vary with time, which is equivalent to the maximum percentage of water adsorbed at long or infinite time. Moisture desorption was then determined in an analogous way by varying the relative humidity from 90 % to 50 % and performing the corresponding weighings.

Reversibility was calculated from the ratio in percent between the amount of water vapor released on desorption and the amount of water adsorbed.

$$q_t(\%) = \frac{m_t - m_0}{m_0} \cdot 100 \qquad \text{Eq. (1)}$$

The porous microstructure of the fired specimens was characterised by means of field-emission gun environmental scanning electron microscope (FEG-ESEM; Quanta 200 FEG, FEI Company) and the determination of pore diameter distributions was performed by mercury intrusion porosimetry and nitrogen gas adsorption. For the former, an automated mercury porosimeter (AutoPore IV 9500, Micromeritics) was used. This equipment records the variation of mercury intrusion volume experienced by the tested sample as a function of the pressure applied on it and transforms the applied pressures into pore diameter values according to Washburn's equation and a mercury-ceramic contact angle of 130º. Thus, a graphical representation of the accumulated intrusion volume as a function of the mean pore diameter analysed is obtained. Nitrogen adsorption/desorption curves were determined with gas adsorption analyser equipment (TriStar 3000, Micromeritics) according to the ISO 9277:2010 standard [28]. Before testing, the samples were dried and subjected to nitrogen stream degassing at 150 °C for 2 hours. The amount of adsorbed nitrogen was measured by a static volumetric method. The specific surface area was calculated according to BET (Brunauer-Emmett-Teller) method by multipoint determination. Pore volume and pore diameter distribution were calculated from the curves according to BJH (Barrett-Joyner-Halenda) method.

3 Results and discussion

3.1 Unfired and fired composition samples characterisation

The chemical composition of the samples tested, expressed as oxides, together with the loss on ignition (LOI) at 1000 ºC are presented in Table 2. The main components are silica (SiO_2) and alumina (Al_2O_3), although in some samples the amounts of iron oxide (Fe_2O_3), calcium (CaO) and magnesium (MgO) stand out with percentages higher than 5 %. The main crystalline structures identified by X-ray diffraction are detailed in Table 3. The major compounds in each composition are underlined in the table, with the main phases that generate porosity in the first place. The presence of calcite in samples C1 and C2, dolomite in samples C2 and C3 and gibbsite in samples C4 and C5 stand out, the remaining phases being similar and common in many ceramic materials manufacture.

Between C1, C2 and C3 there is a difference in the percentage of calcium oxide (CaO) and magnesium oxide (MgO) while C4 and C5 differ in the presence of talc and the amount of alumina (Al_2O_3). Losses on ignition are different for each composition but above 10 % in all cases.

Table 2. Chemical analysis (in wt%) of the five compositions studied in this research

Sample	SiO_2	Al_2O_3	Fe_2O_3	CaO	MgO	Na_2O	K_2O	Others	LOI
C1	57.1	15.5	5.2	6.3	1.7	0.4	3.2	0.5	10.1
C2	29.1	10.5	3.6	18.0	8.9	0.2	2.5	0.7	26.5
C3	51.7	15.7	0.4	7.7	5.6	0.3	1.2	0.5	16.9
C4	32.9	38.9	0.4	0.5	5.7	0.4	0.3	0.3	20.6
C5	28.3	46.0	0.5	0.2	0.3	0.5	1.0	0.8	22.4

Table 3. Mineralogical phases identified by X-ray diffraction in the five compositions studied. The indicated phases only identify the majority phases in each composition

C1	C2	C3	C4	C5
Calcite	Calcite	Dolomite	Gibbsite	Gibbsite
Quartz	Dolomite	Quartz	Quartz	Quartz
Kaolinite	Quartz	Kaolinite	Kaolinite	Kaolinite
Illite	Kaolinite	Illite	Talc	Illite

The physical properties of the fired specimens are shown in Table 4, which details maximum firing temperatures, bulk densities, linear shrinkages and water absorptions. Densities and linear shrinkages differ substantially depending on the nature of each sample, although all the pieces show high porosity with water absorption values close to or higher than 20 %. The high absorption of the pieces corresponding to compositions C2 and C5 stands out, although this is due to different reasons. Thus, on the one hand, composition C2, being a clayey marl with a high carbonate content (more than 40 wt%) gives rise to a high LOI (see Table 2) and, consequently, the fired pieces are very porous. On the other hand, composition C5 with a high aluminium oxide content is still well below its maximum sintering rate temperature at 1120 ºC, also giving rise to very porous pieces.

Table 4. Physical properties of the specimen fired at maximum temperature: bulk density (ρ), linear shrinkage (LS), water absorption (WA) and open porosity (P)

Sample	T (ºC)	ρ (g·cm^{-3})	LS (%)	WA (%)	P (%)
C1	1100	1.78	0.48	18.6	33.1
C2	1080	1.46	3.32	34.6	50.4
C3	1020	1.62	0.15	25.5	41.4
C4	1120	1.74	4.05	22.4	39.1
C5	1120	1.40	4.39	37.3	52.3

3.2 Assessment of humidity regulation capability

Figure 1 shows the moisture adsorption and desorption curves of the pieces at a constant temperature of 23 ºC in 24-hour cycles. Table 5 collects the total incremental amounts of water adsorbed when the relative humidity is varied from 50 % to 90 %, the water vapour released when the humidity is varied from 90 % to 50 % and the percentage of reversibility achieved in the test (desorption/adsorption ratio). Since it is not evident that equilibrium moisture content is reached for samples C4 and C5 within 24 hours, the adsorption test was repeated by increasing the duration to 80 hours. The resulting isotherms are displayed in Figure 2. The highest adsorption corresponds to the pieces of composition C5, which experience an increase in moisture content of about 7 %, moisture content that is higher than corresponding those for low temperature sintered materials with allophane [29]. Sample C4 also adsorbs an appreciable amount of water, with an increase in weight of about 2 % in 24 hours and 2.5 % in 80 hours. The reversibility for both samples is high, with values above 95 %. The remaining samples (C1, C2 and C3) show more discrete water adsorptions, so their potential as materials with moisture regulating functionality is very limited. Samples C2 and C3 have a low reversibility value, so that the material only releases part of the adsorbed water when the relative humidity of the air decreases and the variations in moisture content are not due to adsorption and desorption phenomena by capillary condensation. The moisture regulation of sample C1 is practically negligible.

In all cases, it can be found that the amount of water adsorbed by the pieces is not related to water absorption, i.e., the increase in open porosity does not necessarily improve the

moisture regulating capacity of a material. In addition, when the kinetics of the processes are compared, it can be appreciated that moisture desorption occurs at a faster rate than adsorption. Thus, during desorption, most of the water vapour is released in the first instants and the process is completed in less than 24 hours. During adsorption, a significant amount of water is also adsorbed for the first hours of the test; however, the process continues after 24 hours with more modest variations that follow an asymptotic trend up to the equilibrium value. More than 60 % of the total amount of moisture is adsorbed in time periods of 8 hours and over 90 % of the desorption process is completed in periods of less than 8 hours. The shape of adsorption and desorption curves agrees with literature data, although the relative humidity variations applied during the tests differ between researches [11], [14], [29].

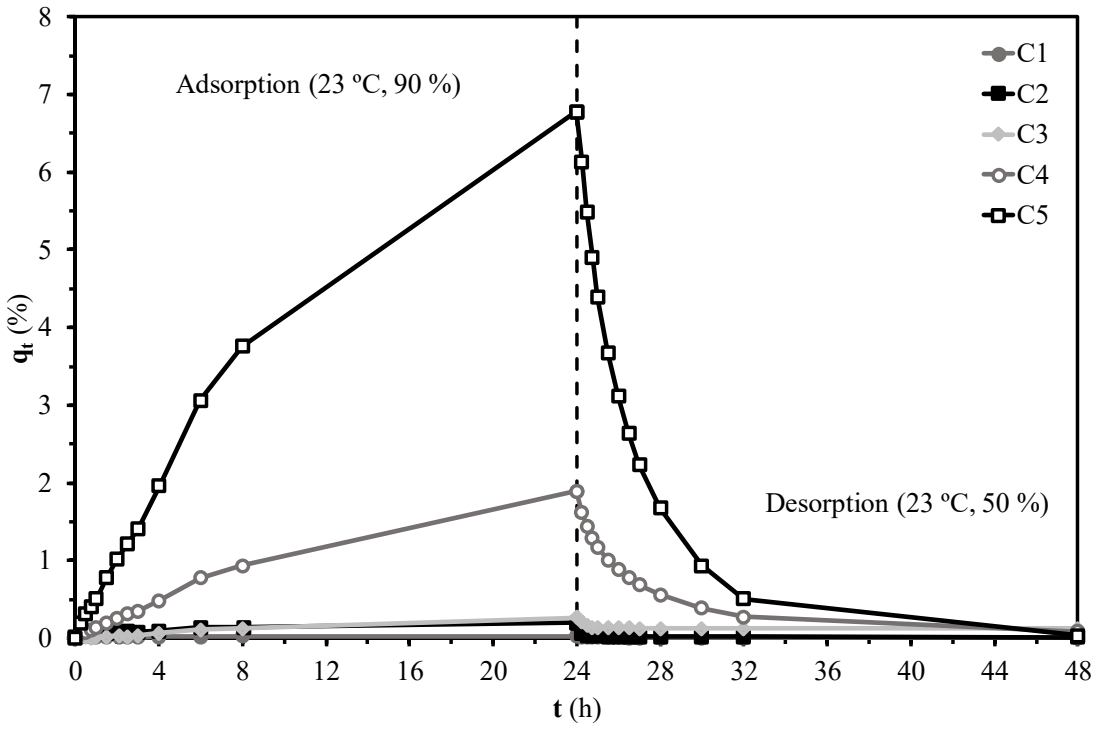

Figure 1. Moisture adsorption and desorption curves in 24-hour cycles

Table 5. Amount of water adsorbed, released during desorption and percentage of reversibility in 24-hour cycles

Sample	Adsorption (%)	Desorption (%)	Reversibility (%)
C1	0.02	0.02	100
C2	0.20	0.19	96
C3	0.27	0.14	54
C4	1.89	1.80	95
C5	6.78	6.75	100

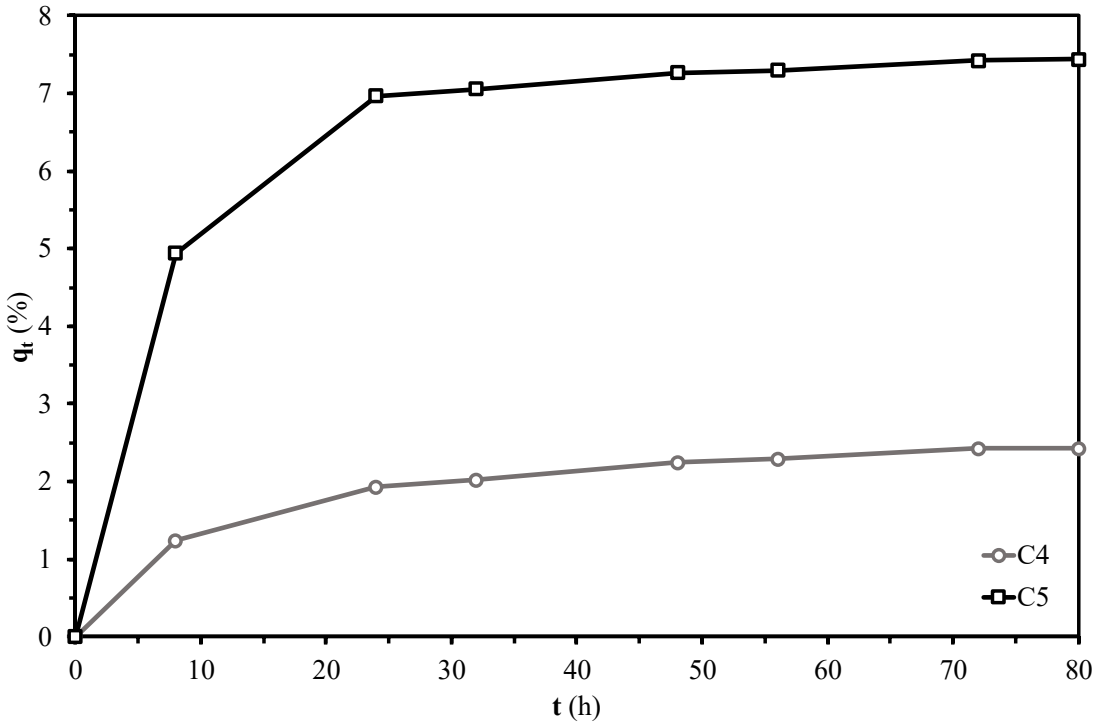

Figure 2. Moisture adsorption curves over longer periods of time for samples C4 and C5

A mathematical model can be performed from the kinetic analysis based on adsorption and desorption isotherms that relate incremental moisture content to time. There are different formulations and mechanisms that describe sorption kinetics in solids, which are usually expressed by the pseudo-first order equation of Lagergren, the pseudo-second order equation and the Elovich equation [30], [31]. Hu et al. [32], have found that the kinetic model based on the pseudo-second order equation adequately fits adsorption and desorption processes in humidity regulating materials such as diatomite. The differential

equation of the pseudo-second order model relates the sorption rate to the difference in incremental moisture content with respect to equilibrium according to equation 2:

$$\frac{dq_t}{dt} = K(q_e - q_t)^2 \qquad \text{Eq. (2)}$$

where q_e is the incremental amount of moisture at equilibrium, q_t is the incremental amount of moisture at a certain time t and K is the pseudo-second order sorption rate constant.

If equation 2 is integrated, it is possible to obtain a representative equation for both adsorption and desorption processes depending on the boundary conditions. For the adsorption step, taking into consideration the boundary conditions $q_t = 0$ at $t = 0$ and $q_t = q_t$ at $t = t$ for moisture adsorption, yields equation 3:

$$\frac{t}{q_t} = \frac{1}{Kq_e^2} + \frac{1}{q_e}t \qquad \text{Eq. (3)}$$

For the desorption step, considering the moisture desorption as a negative adsorption and taking into consideration the boundary conditions $q_t = q_0$ at $t = 0$ and $q_t = q_t$ at $t = t$ results in equation 4:

$$\frac{t}{q_0 - q_t} = \frac{1}{K(q_e - q_0)^2} + \frac{1}{q_e - q_0}t \qquad \text{Eq. (4)}$$

Equation 3 indicates that plotting the ratio t/q_t versus t for adsorption should yield a linear relationship with an equilibrium moisture content q_e and a value of the rate constant K which can be calculated from the slope and the ordinate at the origin respectively. Equation 4 implies a linear relationship too, but of the term $t/(q_0-q_t)$ versus t for desorption, from whose slope and ordinate at the origin q_e and K can also be calculated respectively.

The graphical representation of the fitting results for adsorption isotherms at 24 hours is shown in Figure 3, for desorption isotherms at 24 hours in Figure 4 and for the adsorption at longer times in Figure 5. From all these figures it can be seen a well fit of the experimental data to the pseudo-second order kinetic model. Since the slope correlates inversely with equilibrium moisture content, the lines are ordered according to moisture regulation from lowest to highest, i.e., the steeper lines correspond to the samples with lower moisture regulation while the more horizontal lines belong to the samples with higher moisture regulation capacity.

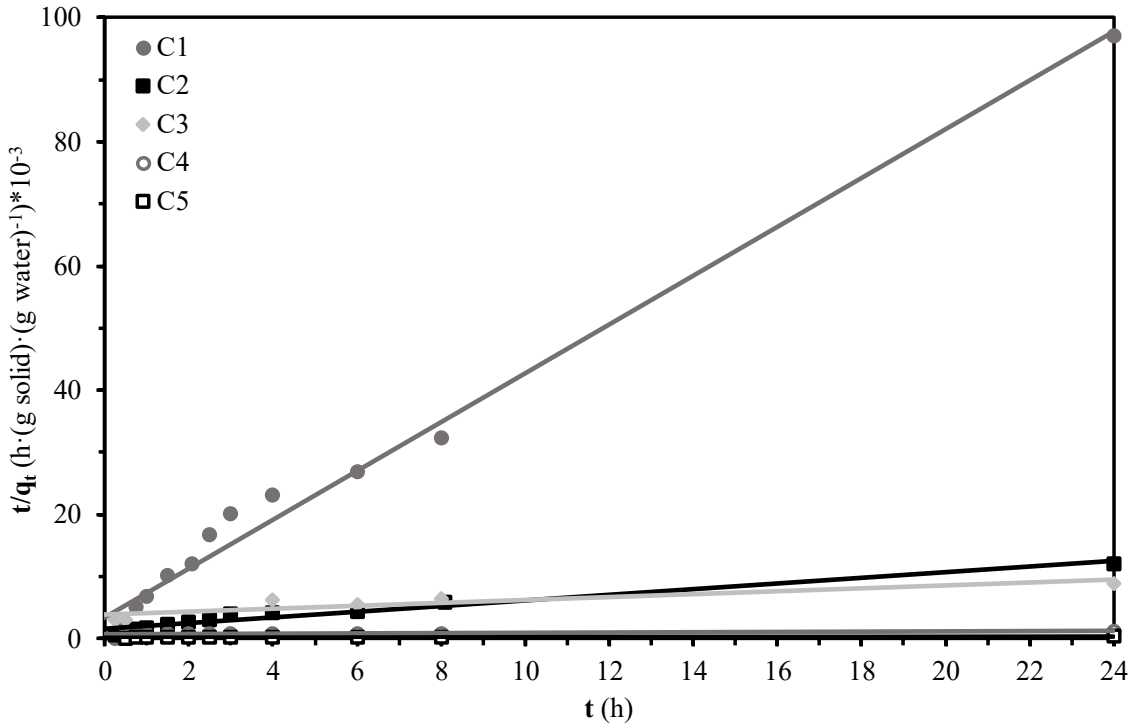

Figure 3. Fitting of adsorption curves to the pseudo-second order kinetic model

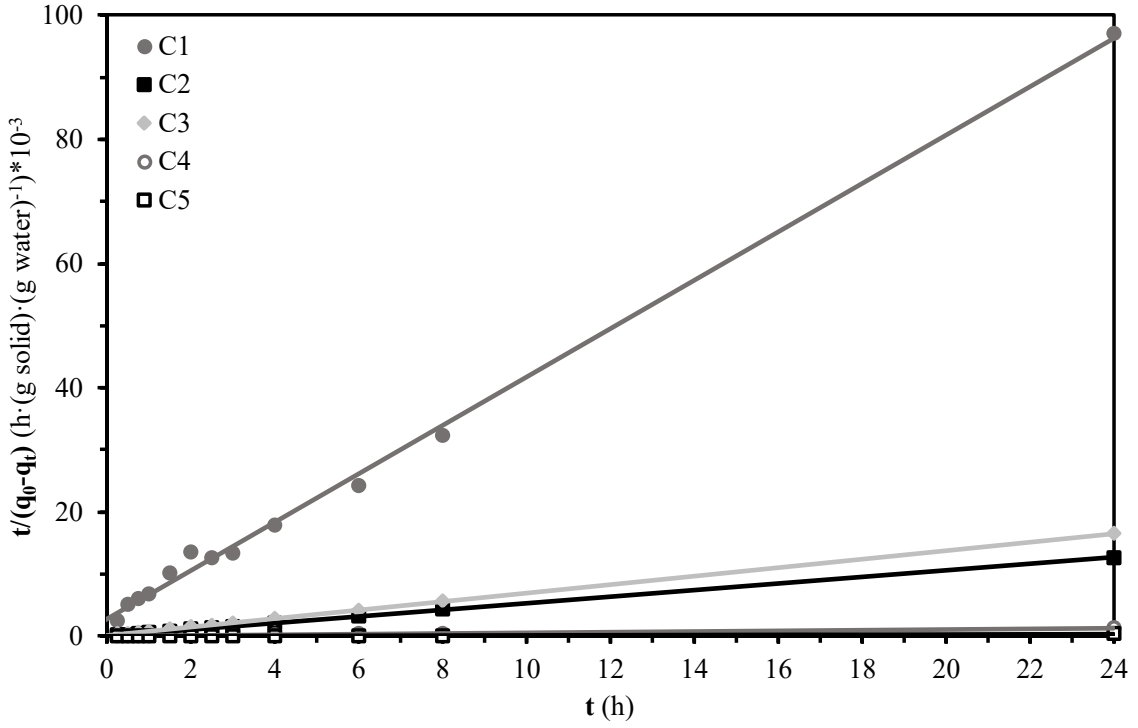

Figure 4. Fitting of desorption curves to the pseudo-second order kinetic model

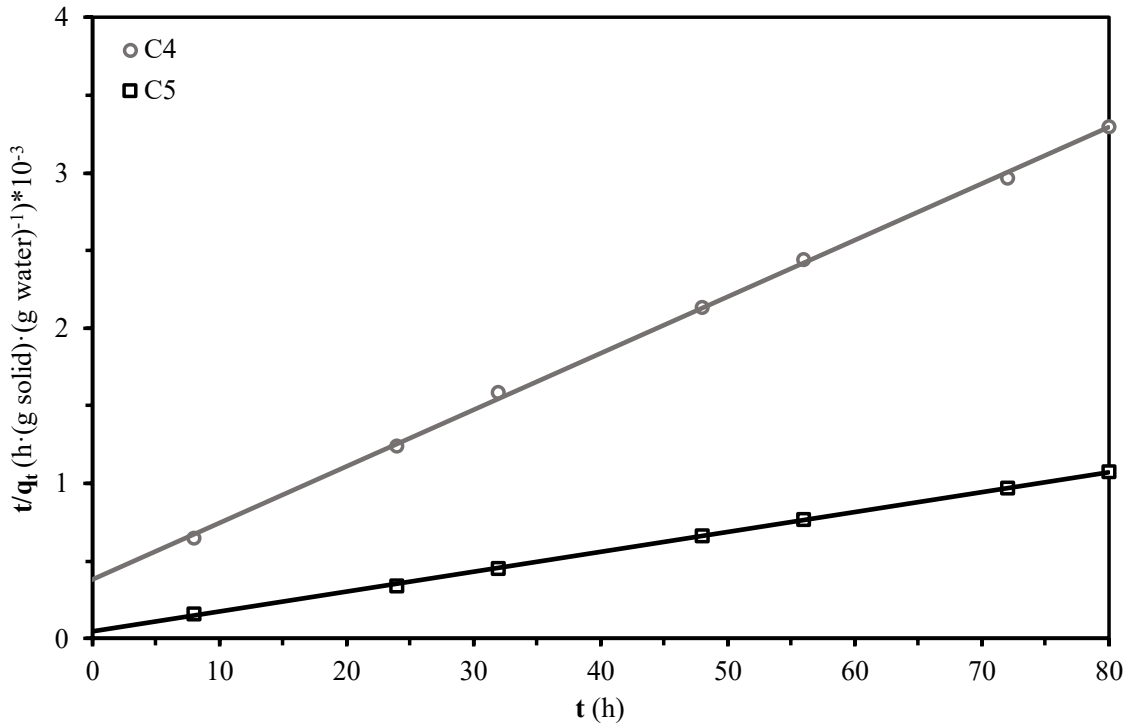

Figure 5. Fitting of desorption curves over longer periods of time to the pseudo-second order kinetic model for samples C4 and C5

The kinetic parameters calculated from the slopes and ordinates at origin are detailed in Table 6. The proper fit of the results is corroborated by correlation coefficients close to unity in most cases. Moreover, the equilibrium moisture quantities calculated from the adsorption process are similar to those obtained from the desorption process, confirming the consistency of the proposed model. The differences in kinetics between adsorption and desorption are also evident with lower rate constants for adsorption compared to desorption. The results are in line with other findings for diatomite materials [32], but the equations for the desorption process have not been used before, since moisture desorption has been in general less analysed and expressions have not been developed applying boundary conditions that do not begin from an equilibrium situation in adsorption, which is a considerable novelty.

When analysing the results of the model fit, it appears that C1 shows hardly any regulation capacity, with a very low equilibrium moisture content. Samples C2 and C3 are distinguished by also low equilibrium moisture content, although greater than C1, and a large rate constant, higher in desorption than in adsorption. This indicates that the materials have some surface adsorption but no or very low diffusion and capillary

condensation, so that the entire amount of adsorbed water is rapidly released when the ambient relative humidity is reduced. On the other hand, the equilibrium humidity of samples C4 and C5 are higher, and the velocity constants are lower. These samples exhibit a more gradual adsorption behaviour in which, in addition to instantaneous adsorption on the surface of the solid, intraparticle diffusion becomes important as occurs in different adsorption processes of other compounds such as dyes or ions [31]. The rate constants for desorption, although higher than for adsorption, are also low because of the pore emptying and diffusion through the porous microstructure that has to take place. Tests over longer periods of time allow the kinetic parameters to be determined more accurately by recording values throughout the process until near equilibrium is reached. Sample C5 shows the highest incremental moisture content at equilibrium.

Table 6. Parameters of the pseudo-second order kinetic model for the samples

Sample	Adsorption (RH = 90 %)			Desorption (RH = 50 %)		
	K ($g \cdot (h \cdot g)^{-1}$)	q_e (%)	R^2	K ($g \cdot (h \cdot g)^{-1}$)	q_e (%)	R^2
C1 (24 h)	4158	0.03	0.989	5441	0.05	0.997
C2 (24 h)	131	0.22	0.959	3639	0.39	1.000
C3 (24 h)	14.3	0.43	0.814	4086	0.41	1.000
C4 (24 h)	0.75	4.33	0.898	30.0	3.82	1.000
C5 (24 h)	0.29	14.0	0.914	6.54	14.2	0.997
C4 (80 h)	3.51	2.74	0.999	-	-	-
C5 (80 h)	3.54	7.79	1.000	-	-	-

3.3 Porous microstructure of samples and its relation to humidity regulation

The porous microstructure conditions the capillary condensation phenomena on which humidity regulation depends. Figure 6 shows the FEG-ESEM images for the different samples. Composition C1 displays a typical microstructure of wall tile, porous ceramic bodies with rounded, sintered pores with a diameter around above 1 μm. In the case of samples C2 and C3, the micrographs show less sintered microstructures comprising smaller pores but without reaching a nanometric scale. On the contrary, composition C4, with a higher humidity regulating capacity, shows a hierarchical microstructure in which larger pores coexist with the presence of alumina rich particle clusters with appearance

of platelets or sheets of very small thickness (marked a in the micrograph) which, although not easily visible in the micrographs, can accommodate large amounts of porosity at the nanometric (mesoporous) scale. Due to the similarity between C4 and C5 microstructures, only C4 microstructure is displayed at two magnifications.

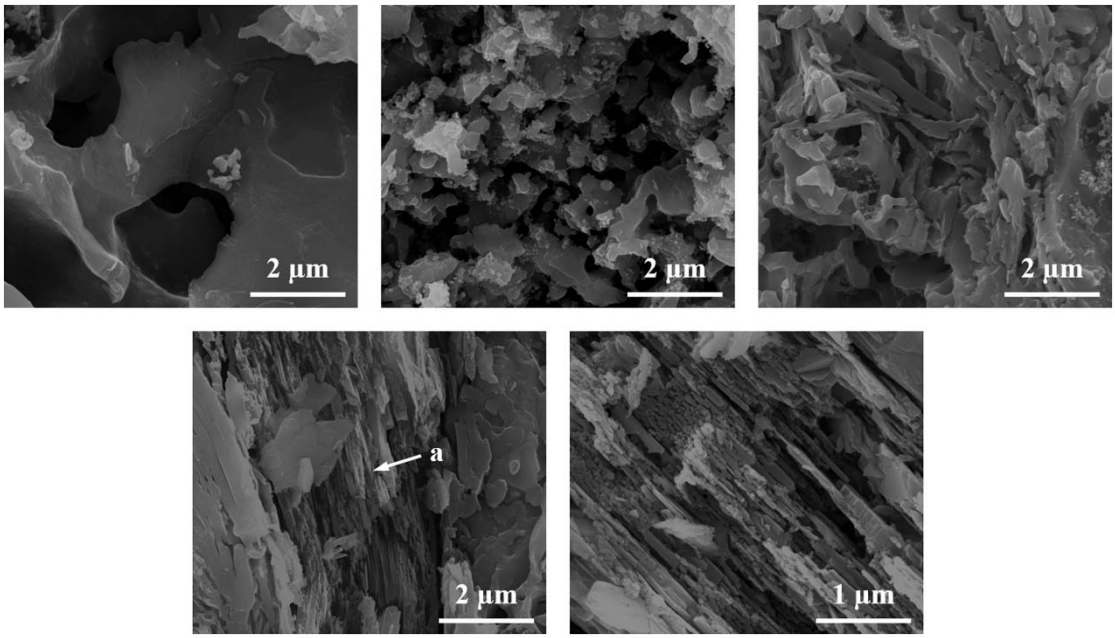

Figure 6. SEM micrographs of the samples fired at the temperatures set out in Table 4; C1, C2 and C3 on top row from left to right and C4 on bottom row at two different magnifications

Regarding the mercury porosimetry analysis, the incremental pore size distributions for the different samples are presented in Figure 7 and the cumulative pore size distributions are shown in Figure 8. The characteristic values of the distributions, including total pore volume, mesopore volume (below 50 nm pores) and percentage of open porosity, are detailed in Table 7. The pore diameter distributions highlight the differences of samples C4 and C5 in relation to the rest, as the hierarchical microstructure is confirmed. These samples present an appreciable amount of small pore sizes with diameters between 0.005 and 0.04 µm (5-40 nm) that provide the ability to regulate humidity to the material. The results also show larger pore sizes for sample C1 with an average pore diameter greater than 1 µm and quite similar distributions for samples C2 and C3, although the total porosity of sample C2 is significantly higher. It is found, therefore, that there is no direct

relationship of humidity regulation with total porosity but with the presence of mesopores (2-50 nm) that allow capillary condensation phenomena. This is in accordance with the results of other studies that address humidity control from materials with porous structures containing mesopores [7], [11], [32]. Mercury porosimetry does not allow discerning the differences in behaviour between samples C4 and C5, being necessary to carry out a more detailed study of the porous nanostructure by nitrogen adsorption.

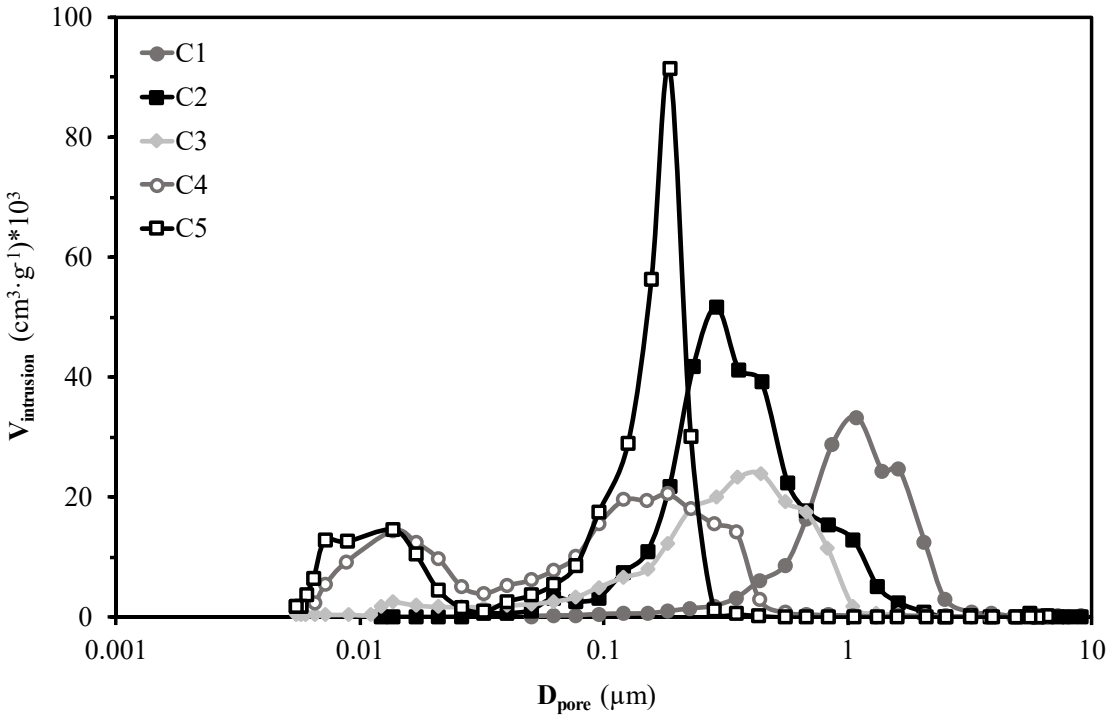

Figure 7. Incremental pore diameter distributions by mercury porosimetry

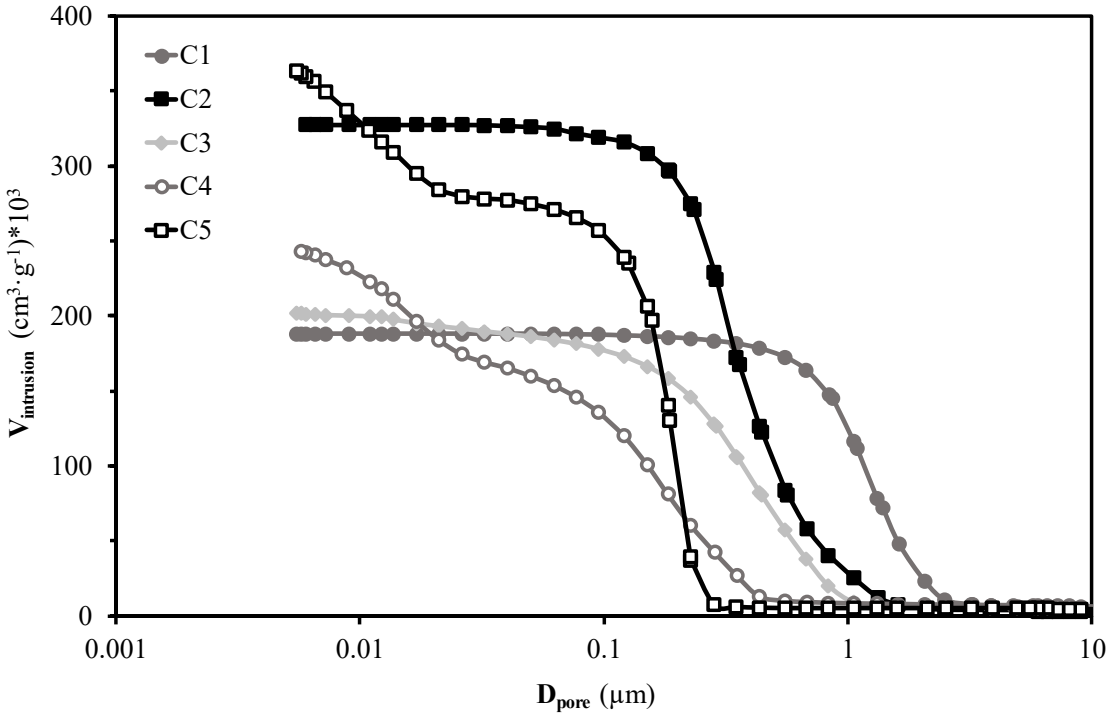

Figure 8. Cumulative pore diameter distributions by mercury porosimetry

Table 7. Characteristic diameters of pore size distribution (d_{16}, d_{50} and d_{84}), total pore volume (V_p), mesopore volume (V_{50}) and percentage of open porosity (P) obtained by mercury porosimetry

Sample	d_{16} (µm)	d_{50} (µm)	d_{84} (µm)	V_p ($cm^3 \cdot g^{-1}$)	V_{50} ($cm^3 \cdot g^{-1}$)	P (%)
C1	1.92	1.20	0.73	0.188	0.000	33.7
C2	0.73	0.36	0.23	0.327	0.001	49.1
C3	0.72	0.37	0.13	0.202	0.016	38.8
C4	0.30	0.12	0.02	0.244	0.084	40.4
C5	0.22	0.16	0.01	0.364	0.089	51.7

The nitrogen adsorption/desorption curves for samples C4 and C5 are shown in Figure 9. The curves display hysteresis according to a Type IV sorption behaviour, typical of materials with mesopores that are filled and emptied by capillary condensation [33]. The volume of nitrogen adsorbed is higher for sample C5.

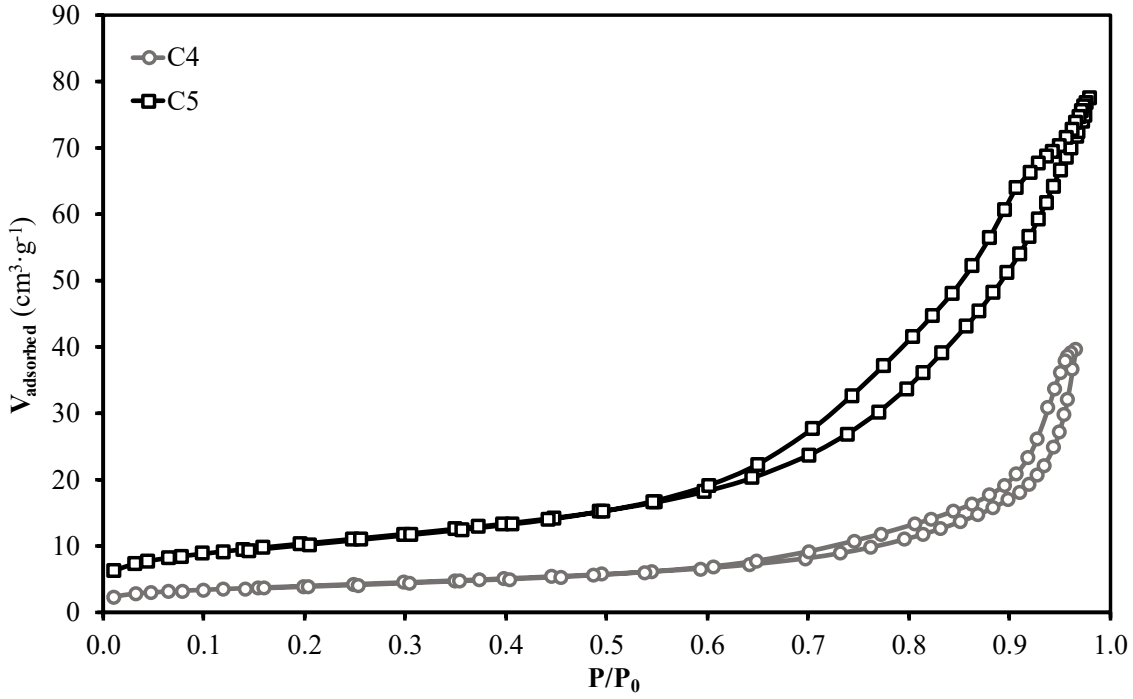

Figure 9. Nitrogen adsorption/desorption isotherms for samples C4 and C5

The specific surface area for samples C4 and C5 determined from the adsorption/desorption curves according to BET method are detailed in Table 8 while the pore size distributions obtained according to BJH method are presented in Figure 10. Table 8 also shows the accumulated pore volume under desorption and the average pore diameter value, calculated as 4V/A where V is the volume and A is the total pore area. The results show the higher specific surface area of sample C5, with a pore size distribution that presents a higher pore volume and a lower mean pore diameter value in the analysed range. Thus, sample C5 has a greater capacity for capillary condensation and, therefore, better humidity regulation functionality in relation to sample C4, probably associated to the higher amount of gibbsite in the starting composition which evolves in nanostructured alumina after the firing process. Several findings indicate that a higher surface area provides more active sites for moisture adsorption and a higher volume of small mesopores facilitates capillary condensation [10], [32], [34]. Moreover, the pore volumes are larger than those determined for allophane materials or mixtures of clays with allophane when the firing temperatures are higher than 1000 ºC, in particular in the case of sample C5 [29]. Pore diameter distributions are similar to the ones described for humidity control materials based on diatomite or volcanic compounds [11].

To clarify the role of the gibbsite in the phase composition of the fired samples, diffractograms obtained by X-ray diffraction are shown in Figure 11. The presence of quartz stands out as the predominant crystallographic phase while the gibbsite has mostly transformed into transition aluminas that contribute to mesoporosity, without developing appreciable α-Al_2O_3 transformation that occurs at temperatures of 1200 °C or higher [35].

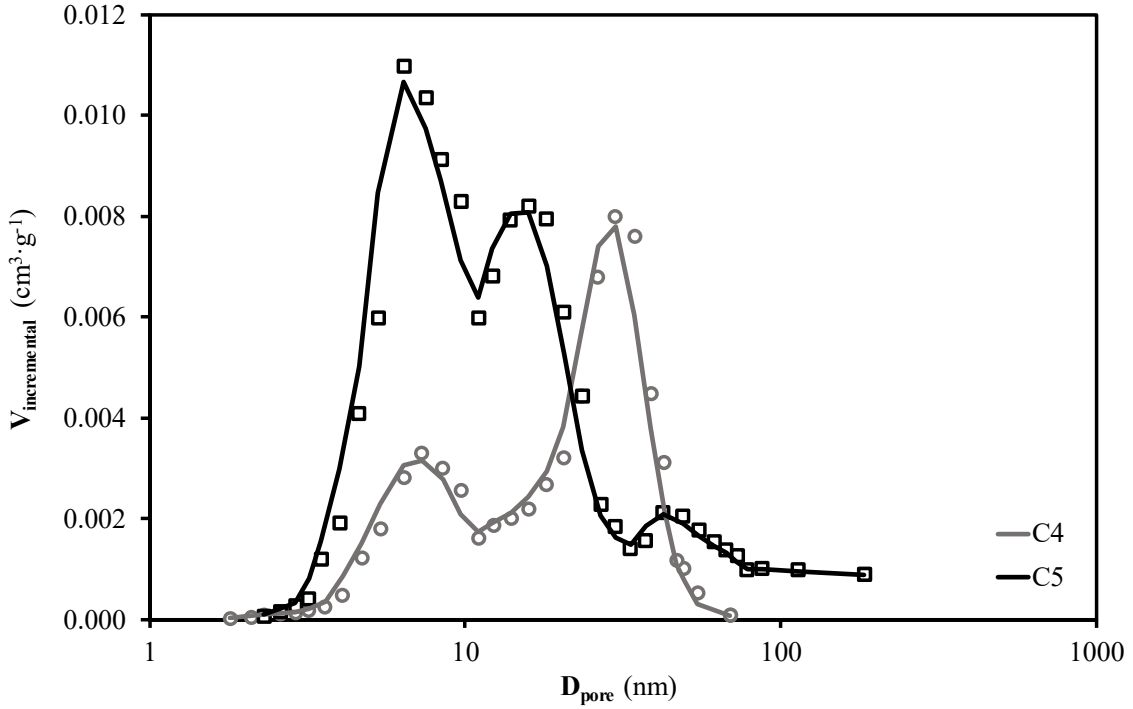

Figure 10. Pore diameter distributions for nitrogen adsorption by BJH method for compositions C4 and C5

Table 8. Specific surface area (S_{BET}), total pore volume accumulated in desorption (V_p) and mean pore diameter (D_p) obtained by nitrogen adsorption for compositions C4 and C5

Sample	S_{BET} ($m^2 \cdot g^{-1}$)	V_p ($cm^3 \cdot g^{-1}$)	D_p (nm)
C4	14	0.062	14.5
C5	37	0.123	10.3

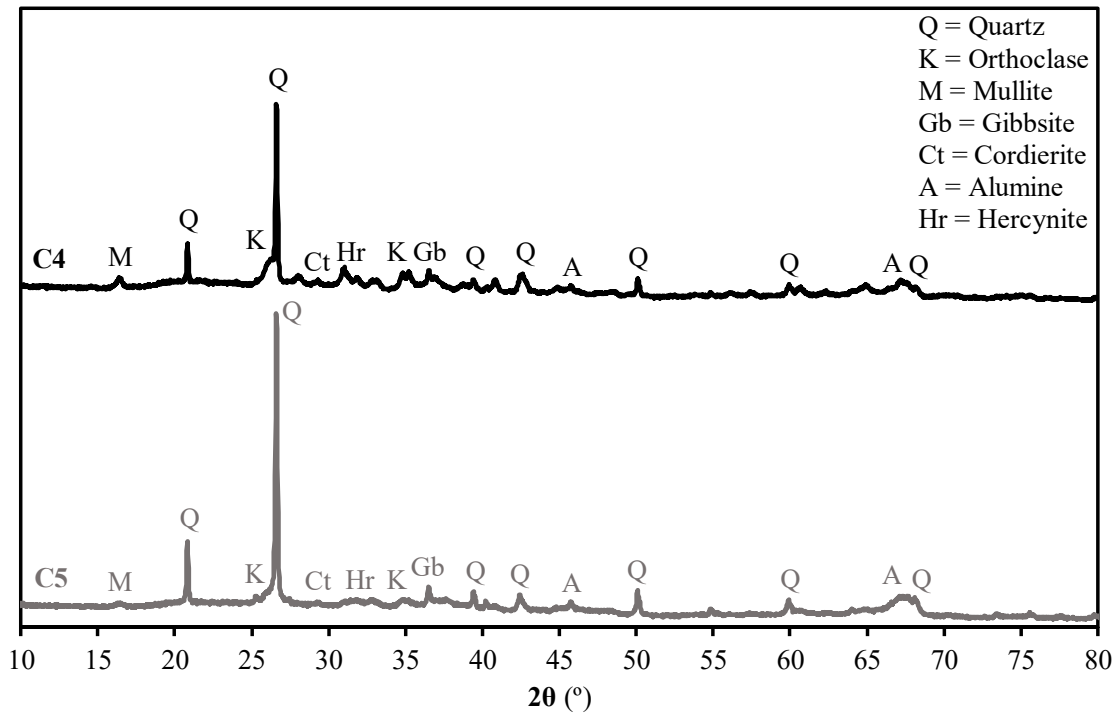

Figure 11. X-ray diffractograms with phase identification for samples C4 and C5

4 Conclusions

Five compositions used in the ceramic industry have been analysed to evaluate their properties for use in tiles with humidity regulation functionality. For this purpose, their chemical and mineralogical composition, the firing properties of pieces sintered from them, the water vapour adsorption and desorption capacities when varying the relative humidity of the environment and the porous nanostructure have been determined by means of SEM analysis, mercury porosimetry and nitrogen gas adsorption.

The pieces of C4 and especially C5 compositions display the best humidity regulation and contain gibbsite in their composition. As a novelty, these compositions are used in the manufacture of common porous ceramics, so that their availability is greater than other special or more specific compositions.

The moisture adsorption and desorption isotherms of the samples follow a pseudo-second order kinetic model, whose equations for moisture desorption have been developed for the first time. From the linear regressions, kinetic parameters (equilibrium moisture content and rate constant) that characterise the behaviour can be determined. Humidity regulation depends on the porous microstructure, mainly the presence of mesopores (2-

50 nm). Adsorption and desorption phenomena are related to the filling and emptying of mesopores by capillary condensation. The amount and size of mesopores defines the humidity regulating capacity of the material. In the absence of mesopores, the remaining porosity has little influence on the humidity regulating capacity.

Although the presence or absence of mesopores can be evidenced by mercury porosimetry, nitrogen adsorption is key for the characterisation since it allows determining specific surface area, total volume of mesopores and mean pore diameter. Sample C5, which shows the best humidity regulation capacity, has the highest specific surface area, the highest mesopore volume and the smallest mean pore diameter.

Acknowledgments

Acknowledging Ministerio de Ciencia e Innovación of Spanish Government and European Regional Development Fund (ERDF) of European Union for the funding received in the framework of RTC-2017-5904-5 CONFORTMA project. Authors are also grateful for the collaboration of the company Vicar in the supply of compositions.

References

[1] V. Loftness, B. Hakkinen, O. Adan, A. Nevalainen, Elements that contribute to healthy building design, Environ. Health Perspect. 115 (2007) 965–970. doi:10.1289/ehp.8988.

[2] W.J. Fisk, Q. Lei-Gomez, M.J. Mendell, Meta-analyses of the associations of respiratory health effects with dampness and mold in homes, Indoor Air. 17 (2007) 284–296. doi:10.1111/j.1600-0668.2007.00475.x.

[3] D. Kong, H. Liu, Y. Wu, B. Li, S. Wei, M. Yuan, Effects of indoor humidity on building occupants' thermal comfort and evidence in terms of climate adaptation, Build. Environ. 155 (2019) 298–307. doi:10.1016/j.buildenv.2019.02.039.

[4] A.V. Arundel, E.M. Sterling, J.H. Biggin, T.D. Sterling, Indirect health effects of relative humidity in indoor environments., Environ. Health Perspect. 65 (1986) 351–361. doi:10.1289/ehp.8665351.

[5] P. Wolkoff, Indoor air humidity, air quality, and health – An overview, Int. J. Hyg. Environ. Health. 221 (2018) 376–390. doi:10.1016/j.ijheh.2018.01.015.

[6] H. Zhang, H. Yoshino, K. Hasegawa, J. Liu, W. Zhang, H. Xuan, Practical

moisture buffering effect of three hygroscopic materials in real-world conditions, Energy Build. 139 (2017) 214–223. doi:10.1016/j.enbuild.2017.01.021.

[7] E.H. Ishida, Channelling the forces of nature – Human and earth conscious materials may create new waves, in: Qualicer, 2004: pp. 3–24.

[8] K.S.W. Sing, R.T. Williams, Historical aspects of capillarity and capillary condensation, Microporous Mesoporous Mater. 154 (2012) 16–18. doi:10.1016/j.micromeso.2011.09.022.

[9] C. Arai, T. Mizutani, Y. Murase, T. Hanakawa, Y. Sano, Measurement of pore distribution by water vapour adsorption, J. Soc. Powder Technol. Japan. 20 (1983) 115–121. doi:10.4164/sptj.20.115.

[10] H. Lan, Z. Jing, J. Li, J. Miao, Y. Chen, Influence of pore dimensions of materials on humidity self-regulating performances, Mater. Lett. 204 (2017) 23–26. doi:10.1016/j.matlet.2017.05.095.

[11] D.H. Vu, K.S. Wang, B.H. Bac, B.X. Nam, Humidity control materials prepared from diatomite and volcanic ash, Constr. Build. Mater. 38 (2013) 1066–1072. doi:10.1016/j.conbuildmat.2012.09.040.

[12] O. Watanabe, H. Fukumizu, H. Ishida, Effect on reduction of harmful substances by using porous material with meso-pores, in: 2005 4th Int. Symp. Environ. Conscious Des. Inverse Manuf., IEEE, 2005: pp. 143–144. doi:10.1109/ECODIM.2005.1619189.

[13] G. Zhang, Y. Liu, S. Zheng, Z. Hashisho, Adsorption of volatile organic compounds onto natural porous minerals, J. Hazard. Mater. 364 (2019) 317–324. doi:10.1016/j.jhazmat.2018.10.031.

[14] H. Maeda, E.H. Ishida, Water vapor adsorption and desorption of mesoporous materials derived from metakaolinite by hydrothermal treatment, Ceram. Int. 35 (2009) 987–990. doi:10.1016/j.ceramint.2008.04.007.

[15] O.F. Osanyintola, C.J. Simonson, Moisture buffering capacity of hygroscopic building materials: Experimental facilities and energy impact, Energy Build. 38 (2006) 1270–1282. doi:10.1016/j.enbuild.2006.03.026.

[16] K. Wada, The distinctive properties of andosols, in: Adv. Soil Sci. Vol. 2, Springer, New York, NY, 1985: pp. 173–229. doi:10.1007/978-1-4612-5088-3_4.

[17] H. Fukumizu, S. Yokoyama, Study on a new humidity controlling material porous

soil “allophane” – Evaluation of humidity controlling performance in practical houses, Resour. Process. 52 (2005) 59–64. doi:10.4144/rpsj.52.59.

[18] N.M.M. Ramos, J.M.P.Q. Delgado, V.P. de Freitas, Influence of finishing coatings on hygroscopic moisture buffering in building elements, Constr. Build. Mater. 24 (2010) 2590–2597. doi:10.1016/j.conbuildmat.2010.05.017.

[19] M.P. Gómez-Tena, M.A. Bengochea, E. Sánchez, L. Guaita, C. Machí, Development of ceramic formulations with humidity-regulating capability for environmental comfort, in: Qualicer, 2012: pp. 1–14.

[20] A. El-Turki, R.J. Ball, S. Holmes, W.J. Allen, G.C. Allen, Environmental cycling and laboratory testing to evaluate the significance of moisture control for lime mortars, Constr. Build. Mater. 24 (2010) 1392–1397. doi:10.1016/j.conbuildmat.2010.01.019.

[21] F. Ohashi, M. Maeda, K. Inukai, M. Suzuki, S. Tomura, Study on intelligent humidity control materials: Water vapor adsorption properties of mesostructured silica derived from amorphous fumed silica, J. Mater. Sci. 34 (1999) 1341–1346. doi:10.1023/A:1004510417593.

[22] Y. Tomita, R. Takahashi, S. Sato, T. Sodesawa, M. Otsuda, Humidity control ability of silica with bimodal pore structures prepared from water glass, J. Ceram. Soc. Japan. 112 (2004) 491–495. doi:10.2109/jcersj.112.491.

[23] H.S. Yang, H.J. Kim, H.J. Park, B.J. Lee, T.S. Hwang, Water absorption behavior and mechanical properties of lignocellulosic filler-polyolefin bio-composites, Compos. Struct. 72 (2006) 429–437. doi:10.1016/j.compstruct.2005.01.013.

[24] B. Zhou, Z. Chen, Experimental study on the hygrothermal performance of zeolite-based humidity control building materials, Int. J. Heat Technol. 34 (2016) 407–414. doi:10.18280/ijht.340309.

[25] J. Zheng, J. Shi, Q. Ma, X. Dai, Z. Chen, Experimental study on humidity control performance of diatomite-based building materials, Appl. Therm. Eng. 114 (2017) 450–456. doi:10.1016/j.applthermaleng.2016.11.203.

[26] F. Caturla, M. Molina-Sabio, F. Rodriguez-Reinoso, Adsorption-desorption of water vapor by natural and heat-treated sepiolite in ambient air, Appl. Clay Sci. 15 (1999) 367–380. doi:10.1016/S0169-1317(99)00030-7.

[27] M.J. Lee, H.J. Lee, K. Kim, H.J. Hwang, Fabrication of humidity control ceramics

from drinking-water treatment sludge and Onggi soil, J. Korean Ceram. Soc. 53 (2016) 362–366. doi:10.4191/kcers.2016.53.3.362.

[28] ISO 9277:2010. Determination of the specific surface area of solids by gas adsorption — BET method, (2010).

[29] O. Watanabe, H. Fukumizu, E.H. Ishida, Development of an autonomous humidity controlling building material by using mesopores, in: Qualicer, 2008: pp. 19–29.

[30] Y.S. Ho, G. McKay, A comparison of chemisorption kinetic models applied to pollutant removal on various sorbents, Process Saf. Environ. Prot. 76 (1998) 332–340. doi:10.1205/095758298529696.

[31] F.C. Wu, R.L. Tseng, R.S. Juang, Kinetic modeling of liquid-phase adsorption of reactive dyes and metal ions on chitosan, Water Res. 35 (2001) 613–618. doi:10.1016/S0043-1354(00)00307-9.

[32] Z. Hu, S. Zheng, Z. Sun, Y. Chen, Y. Yan, Influence of pore structure on humidity control performance of diatomite, Sci. Technol. Built Environ. 23 (2017) 1305–1313. doi:10.1080/23744731.2017.1317576.

[33] K. Sing, The use of nitrogen adsorption for the characterisation of porous materials, in: Colloids Surfaces A Physicochem. Eng. Asp., 2001: pp. 3–9. doi:10.1016/S0927-7757(01)00612-4.

[34] D.H. Vu, K.S. Wang, B.H. Bac, Humidity control porous ceramics prepared from waste and porous materials, Mater. Lett. 65 (2011) 940–943. doi:10.1016/j.matlet.2011.01.006.

[35] I.N. Bhattacharya, S.C. Das, P.S. Mukherjee, S. Paul, P.K. Mitra, Thermal decomposition of precipitated fine aluminium trihydroxide, Scand. J. Metall. 33 (2004) 211–219. doi:10.1111/J.1600-0692.2004.00686.X.